Geophysical Research Letters

RESEARCH LETTER
10.1029/2020GL089997

Key Points:
- Numerical Weather Prediction models use a master turbulence length scale linked to the characteristic wavelength of energy-containing eddies
- A relation predicting variations of this wavelength with atmospheric stability is derived
- Predictions agree with experiments and offer a new perspective on return-to-isotropy approaches

Supporting Information:
- Supporting Information S1

Correspondence to:
A. Ayet,
alex.ayet@normalesup.org

Citation:
Ayet, A., & Katul, G. G. (2020). Scaling laws for the length scale of energy-containing eddies in a sheared and thermally stratified atmospheric surface layer. *Geophysical Research Letters*, *47*, e2020GL089997. https://doi.org/10.1029/2020GL089997

Received 29 JUL 2020
Accepted 5 NOV 2020
Accepted article online 16 NOV 2020

Scaling Laws for the Length Scale of Energy-Containing Eddies in a Sheared and Thermally Stratified Atmospheric Surface Layer

A. Ayet[1,2] **and G. G. Katul**[3]

[1]Ifremer, CNRS, IRD, Université de Bretagne Occidentale/Laboratoire d'Océanographie Physique et Spatiale (LOPS), IUEM, Brest, France, [2]LMD/IPSL, CNRS, École Normale Supérieure, PSL Research University, Paris, France, [3]Nicholas School of the Environment, Duke University, Durham, NC, USA

Abstract In the atmospheric surface layer (ASL), a characteristic wavelength marking the limit between energy-containing and inertial subrange scales can be defined from the vertical velocity spectrum. This wavelength is related to the integral length scale of turbulence, used in turbulence closure approaches for the ASL. The scaling laws describing the displacement of this wavelength with changes in atmospheric stability have eluded theoretical treatment and are considered here. Two derivations are proposed for mildly unstable to mildly stable ASL flows one that only makes use of normalizing constraints on the vertical velocity variance along with idealized spectral shapes featuring production to inertial subrange regimes, while another utilizes a co-spectral budget with a return-to-isotropy closure. The expressions agree with field experiments and permit inference of the variations of the wavelength with atmospheric stability. This methodology offers a new perspective for numerical and theoretical modeling of ASL flows and for experimental design.

Plain Language Summary Turbulent flows in the atmosphere are composed of a large number of eddies whose sizes vary from kilometers to fractions of millimeters. The energy content in the vertical direction associated with each eddy size dictates the overall ability of turbulent motion to mix and transport particles (such as seeds, pollen, or spores), gases (such as carbon dioxide, ozone, methane, and isoprene), energy (such as latent and sensible heat), and momentum from or to the underlying surface. Despite this multiplicity of eddy sizes, numerous experiments and simulation studies have shown that an effective or dominant eddy size may be sufficient to represent the overall mixing and transport properties of turbulent flows. This finding is a cornerstone to representing the effects of turbulence on transport in Numerical Weather Prediction models. The work here explores how surface heating or cooling (i.e., near-surface atmospheric stability) regulates this dominant or effective eddy size. The derivation makes use of well-established constraints on the overall turbulent kinetic energy in the vertical direction and highlights the parameters dictating this regulation.

1. Introduction

Close to the ground, in the so-called atmospheric surface layer (ASL), shear and buoyancy forces impact many flow statistics including the distribution of turbulent kinetic energy (TKE) among eddy sizes (Kaimal & Finnigan, 1994). This is apparent in the spectrum of the vertical velocity $E_{ww}(k)$ (k is the streamwise wavenumber related to an inverse eddy size) which exhibits a two-regime behavior, valid for a mildly stable to unstable atmosphere (Kaimal & Finnigan, 1994; Wyngaard, 2010, pages 42 and 216, respectively, and references therein). This behavior is exemplified in Figure 1a for flows above several surfaces and a near-neutral stratification. At large k (small scales), $E_{ww}(k)$ follows an approximate $k^{-5/3}$ law predicted by Kolmogorov's theory (Kolmogorov, 1941) for locally homogeneous and isotropic turbulence (the inertial subrange). For low k (in the so-called production subrange), $E_{ww}(k)$ follows an approximate k^0 law, presumed to occur because the surface leads to "splashing" (redistribution) of energy across scales (see, e.g., Ayet, Katul, et al., 2020; Hoxey & Richards, 1992; Hunt & Carlotti, 2001).

A key variable in the description of this two-regime behavior, and hence of the near-surface $E_{ww}(k)$, is the wavenumber k_p of the transition between production and inertial subranges. In fact, k_p^{-1} is proportional

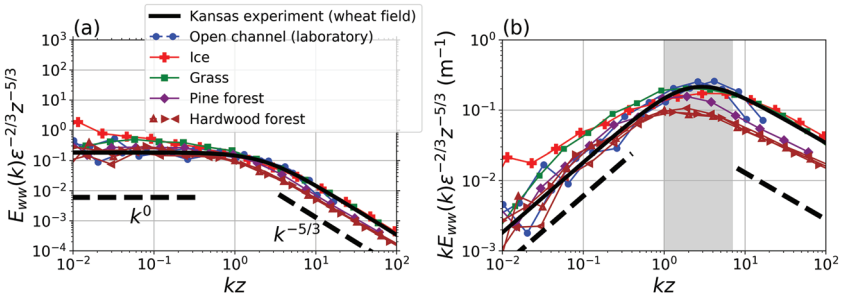

Figure 1. Illustrative figure showing the existence of a transition wavenumber in the *near-neutral ASL*. (a) Normalized vertical velocity spectra and (b) its premultiplied version (i.e., multiplied by k) as a function of the normalized wavenumber. In the normalization factor $\epsilon^{2/3}z^{5/3}$, ϵ is the TKE dissipation rate, and z is the measurement height. In (a) dashed lines show the existence of two regimes, separated by a transition wavenumber k_p, apparent in (b) where it spans one decade around $1/z$ (gray shadings) for the data shown here. The experiments and data sources span forests, grassland, ice sheets, and canonical smooth walls. The post-processing and data sources are described elsewhere (Kaimal et al., 1972; Katul & Chu, 1998; Katul et al., 2012, 2016; Katul, Hsieh, Kuhn, et al., 1997; Katul, Hsieh, & Sigmon, 1997) and are not repeated here. Only the Kansas data are used in the rest of the analysis since the other data here are available for near-neutral conditions only and are solely used to illustrate near-neutral conditions above various types of surfaces.

to the characteristic scale of energy-containing eddies close to the surface and to the integral length scale of turbulence (Katul et al., 2007; Townsend, 1980). As such, its value is needed in closure schemes such as the Mellor-Yamada scheme (Mellor & Yamada, 1982) used in numerical weather prediction models and for Large Eddy Simulations. In both cases, an integral length scale (also called master length scale) is required (e.g., Mellor & Yamada, 1982; Redelsperger et al., 2001; Rodier et al., 2017). Furthermore, knowledge of the physics upon which k_p depends provides insights into the energy redistribution mechanisms in the ASL. Indeed, k_p separates (small scale) isotropic and (large scale) anisotropic motions, and the difference between those motions is grounded, among others, in how energy is redistributed among the different turbulent components. In the abovementioned numerical models, these mechanisms are modeled through return to isotropy closure schemes (Abid & Speziale, 1993; Canuto et al., 2001; Cuxart et al., 2000; Drobinski et al., 2007; Launder et al., 1975; Lumley & Newman, 1977; Mellor & Yamada, 1982), whose validity has been recently questioned for a sheared and stratified ASL (Ayet, Katul, et al., 2020).

Finally, knowledge of the transition wavenumber is also essential for other geophysical applications involving $E_{ww}(k)$. Two examples are singled out: the first is the determination of the effectiveness of the vertical dispersion of scalars, or Lagrangian stochastic modelling of turbulence, which both rely on the vertical velocity variance $\sigma_w^2 = \int_0^\infty E_{ww}(k)dk$ (e.g., Taylor, 1922) along with a characteristic length or timescale. The second example are co-spectral budgets and related phenomenological models describing turbulent momentum transport in the ASL (Gioia et al., 2010; Katul et al., 2011, 2014). In those models, the vertical velocity spectrum is prescribed under an idealized form, and the value of the transition wavenumber is key to recover the flow statistics over a flat wall (Katul et al., 2011, 2013, 2014), a rough channel (Bonetti et al., 2017), or ocean surface waves (Ayet, Chapron, et al., 2020).

For the neutral conditions of Figure 1, the transition wavenumber k_p is expected to scale as $1/z$, where z is the distance from the surface, due to energy-containing eddies being attached to the latter (Townsend, 1980). This is exemplified in Figure 1b in which k_p can be determined as the wavenumber of the peak of the so-called "premultiplied spectrum" $kE(k)$. The decade of values spanned by the neutral k_p (gray shadings in Figure 1b) shows that uncertainties remain about the exact value of the proportionality coefficient. The exact value depends, among others, on the geometrical properties of the surface.

In this contribution, this uncertainty is not the main focus. What is sought are variations of the transition wavenumber with shear and buoyancy forces, whose ratio is related to the atmospheric stability parameter. Indeed, starting from the historical Kansas and Minnesota experiments, measurements have revealed robust variations of k_p with atmospheric stability (see, e.g., Figure 4 of Kaimal et al., 1972). Those *relative* variations of k_p with respect to its neutral value are key for the applications cited above, since they determine how the various ASL turbulent processes are influenced by the presence of buoyancy (e.g., the energy redistribution mechanisms; see Ayet, Katul, et al., 2020; Bou-Zeid et al., 2018). This is also a first step towards

understanding the variations of those processes due to other external parameters, for example, fixed roughness elements (Bonetti et al., 2017) or ocean surface waves (Ayet, Chapron, et al., 2020). In addition to the aforementioned applications, the relative variations of k_p with stability have been recently used to explain the shape of the stability correction functions to the log-law mean velocity profile in stratified atmospheric flows (Katul et al., 2011) with caveats partly associated with the assumed variations of k_p with stability (Li et al., 2016; Salesky et al., 2013). Undoubtedly, there is a need for expressions that predict the displacement of k_p with changes in atmospheric stability. To date, no theoretical expression explaining this displacement exists, and this knowledge gap frames the scope of this work.

Two links between the spectral and bulk properties of turbulence are used to provide a constraint on k_p and its variation with the dimensionless stability parameter for mildly stable and unstable conditions (those exclude free convective and very stable conditions where turbulence may be patchy). The expressions derived provide means of estimating the transition wavenumber from bulk quantities of the flow in the ASL. These are then tested with published data sets collected in the ASL (including the weighty Kansas and Minnesota experiments). The expressions also explicitly account for the filtering properties of the instruments, should they be needed.

2. Theory

2.1. Definitions and Nomenclature

A turbulent flow within the ASL is considered with u', v', w', and T' defining the three instantaneous turbulent velocity components in the streamwise (x), cross-stream (y), and vertical (z) directions and the turbulent air temperature fluctuations. These fluctuations have zero-mean so that $\overline{u'} = \overline{v'} = \overline{w'} = \overline{T'} = 0$, where overline indicates time (or ensemble) averaging. Stability dependence of bulk flow statistics and spectral properties of the ASL are routinely expressed in the context of Monin-Obukhov Similarity Theory (MOST, Foken, 2006; Monin & Obukhov, 1954). This similarity theory considers a stationary and planar homogeneous flow without subsidence and turbulent flux transport so that the TKE budget is given by

$$\epsilon = u_*^2 \frac{dU}{dz} + \frac{g}{T_a}\overline{w'T'}, \tag{1}$$

where ϵ is, again, the mean TKE dissipation rate, $-u_*^2 = \overline{u'w'}$ is the turbulent momentum flux (u_* is the friction velocity), $\overline{w'T'}$ is the turbulent sensible heat flux, U is the mean velocity, T_a is the mean air temperature, and g is the gravitational acceleration. Equation 1 can also be rearranged to introduce MOST dimensionless quantities:

$$\epsilon = \frac{u_*^3}{\kappa z}\left[\phi_m(\zeta) - \zeta\right], \tag{2}$$

where $\zeta = z/L$ is the stability parameter, $L = -u_*^3(\kappa g \overline{w'T'}/T_a)^{-1}$ is the Obukhov length, $\kappa = 0.4$ is the von Kármán constant, and $\phi_m(\zeta)$ is the so-called stability correction function for the mean velocity profile, defined below. The ASL is labeled as moderately unstable when $-2 < \zeta < -0.1$, near neutral when $|\zeta| \leq 0.1$, and stable when $0.1 < \zeta < 1$. Conditions where the ASL is in forced ($-5 < \zeta < 2$) or free ($\zeta > -5$) convection (Kader & Yaglom, 1990) or very stable conditions ($\zeta \geq 1$, where the flux Richardson number reaches a maximum; see Grachev et al., 2013; Katul et al., 2014; Li et al., 2016) are outside the scope of the present work. In the following, the analysis is restricted to $-2 < \zeta < 1$.

Within MOST, $\phi_m(\zeta)$ and the dimensionless vertical velocity variances are

$$\phi_m(\zeta) = \frac{\kappa z}{u_*}\frac{dU}{dz}, \quad \phi_w(\zeta) = \frac{\sigma_w^2}{u_*^2}, \tag{3a,b}$$

where $\sigma_w^2 = \overline{w'^2}$. The balance in equation 1 and the validity of the scaling used for MOST stability correction functions (ϕ_m and ϕ_w) are expected to hold for the range of ζ corresponding to mildly stable to unstable conditions, as demonstrated by a number of ASL experiments (Charuchittipan & Wilson, 2009; Hsieh & Katul, 1997; Salesky et al., 2013).

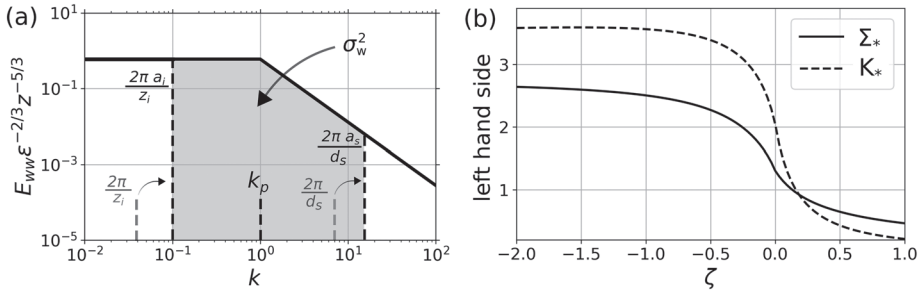

Figure 2. (a) Idealized $E_{ww}(k)$ spectrum (solid line) and key wavenumbers used in the model (dashed lines), for $z = 1$ m and $k_p = 1/z$. In the spectral link (equations 4 and 9), the spectrum is integrated between two finite bounds, and the integration area, corresponding to the measured σ_w^2, is shown as a gray shading. (b) Left-hand side of equations 6 (dimensionless variance Σ_*, solid line) and (10) (dimensionless turbulent viscosity K_*, dashed line) as a function of stability.

2.2. A Spectral Link Approach

In this Letter, the normalization condition for the one-dimensional spectrum of vertical velocity $E_{ww}(k)$ is exploited to arrive at expressions for $k_p z$. The measured σ_w^2 is linked to $E_{ww}(k)$ using

$$\sigma_w^2 = \int_{2\pi a_i/z_i}^{2\pi a_s/d_s} E_{ww}(k)dk, \tag{4}$$

where σ_w^2 is routinely measured using sonic or acoustic Doppler anemometers. Because scales in the flow are finite in any experiment, the spectrum is integrated between two wavelengths (gray shading in Figure 2a): (i) a fraction a_i of the wavelength of the largest energetic scale $2\pi/z_i$, where z_i is the height of the boundary layer; (ii) a fraction of a_s of the wavelength sampled by the measuring device $2\pi/d_s$. In the case of sonic anemometery common to ASL field experiments, d_s is the path length between transducers (of the order of 0.1 m for many commercial anemometers). For a given measurement height z, it is assumed that $d_s < z < z_i$. The proportionality constant a_i accounts for the fact that, due to a finite sampling period, not all the large scales of the flow might be sampled. In contrast, the proportionality constant a_s reflects the effect of unresolved eddies (smaller than d_s) on the measured small-scale spectrum of turbulence. This high-wavenumber energy correction results, among others, from the choice of instrument averaging (Moore, 1986). The quantities $2\pi a_i/z_i$ and $2\pi a_s/d_s$ are hence the *effective* wavelengths in between which the spectrum is effectively sampled.

To extract information about k_p, an idealized spectral shape for $E_{ww}(k)$ is considered and is given under its normalized form by

$$\frac{E_{ww}(k)}{\epsilon^{2/3}z^{5/3}} = \begin{cases} C_{ww}(zk_p)^{-5/3}k^0, & k \le k_p \\ C_{ww}(zk)^{-5/3} & k > k_p \end{cases}, \tag{5}$$

where $C_{ww} = 0.65$ is the Kolmogorov constant for the vertical velocity energy spectrum (Saddoughi & Veeravalli, 1994). This spectrum consists of the two regimes mentioned in section 1 (dashed lines in Figure 1a and solid line in Figure 2a): (i) the inertial subrange for $k > k_p$ (Kolmogorov, 1941); (ii) the production range for $k \le k_p$, whose spectral constant is determined by requiring continuity (but not smoothness) with regime (i). Under neutral conditions, the transition wavenumber is inversely proportional to the measurement height so that $k_p z = C_1$ (Townsend, 1980). As mentioned in section 1, the focus of the Letter is on the displacement of k_p with ζ from its neutral value, labeled $k_p(0)$ (for $\zeta = 0$).

The idealized spectral shapes defined in equation 5 agree with numerous measurements published in the literature (Kader & Yaglom, 1991; Kaimal & Finnigan, 1994; Katul et al., 2012), and only few examples are shown in Figure 1 to illustrate their existence and general features for different surface covers. The measurements reported here are for different types of ASL experiments: flow over an ice sheet (Katul et al., 2016), grass (Katul, Hsieh, & Sigmon, 1997), a pine forest (canopy height 14 m), and a hardwood forest (canopy height 28 m) (Katul, Hsieh, Kuhn, et al., 1997). For reference, results for an open channel flow above a smooth stainless steel surface at two differing bulk Reynolds numbers are also featured (Katul & Chu, 1998). The spectra in the ASL presented here have been selected for near-neutral conditions and for runs where stationary conditions prevailed over extended periods of time (>3,600 s). For $-2 < \zeta < 1$, the idealized spectral

shapes for vertical velocity spectra roughly hold but with a displaced k_p (e.g., Figure 4 of Kaimal et al., 1972). Note that this is not the case for highly unstable or very stable stability conditions (not considered here), as shown by several long-term experiments (Grachev et al., 2013; Kader & Yaglom, 1991). With respect to more sophisticated models of the spectra (see, e.g., Tchen, 1953; Panchev, 1971), the idealized spectral shapes of equation 5 retain the essential feature needed in the present work: the existence of two regimes separated by the transition wavenumber k_p.

To obtain an expression for zk_p, equation 5 is inserted into equation 4, yielding

$$\Sigma_* = (zk_p)^{-2/3}\left\{\left[1-\frac{2\pi a_i z}{z_i}(zk_p)^{-1}\right]+\frac{3}{2}\left[1-\left(\frac{d_s}{2\pi a_s z}\right)^{2/3}(zk_p)^{2/3}\right]\right\}, \tag{6}$$

where z has been introduced to normalize length scales (as in equation 5) and $\Sigma_* = \sigma_w^2(C_{ww}z^{2/3}\epsilon^{2/3})^{-1}$ is a dimensionless vertical velocity variance that depends on the bulk characteristics of the turbulent flow, and hence, only on atmospheric stability (discussed in section 2.4). Equation 6 has two terms balancing Σ_* on the right-hand side (RHS): (i) contributions from the production subrange (first term) and from the inertial subrange (second term). Solving this expression for externally supplied z_i, d_s, and Σ_* as well as estimates of a_i and a_s determines zk_p.

2.3. A Co-Spectral Budget Approach

An alternative model for determining $k_p z$ is now proposed based on a different set of assumptions. It relies on the normalization condition of the co-spectrum of vertical and horizontal velocity fluctuations $F_{uw}(k)$

$$-\overline{u'w'} = \int_{2\pi a_i/z_i}^{2\pi a_s/d_s} F_{uw}(k)dk. \tag{7}$$

Using the same idealized flow conditions as those of equation 1, $F_{uw}(k)$ follows a co-spectral budget given as (Bos et al., 2004; Katul et al., 2013; Panchev, 1971)

$$\frac{\partial F_{uw}(k)}{\partial t} = 0 = \frac{dU}{dz}E_{ww}(k) - \frac{C_R}{\tau(k)}F_{uw}(k) - C_l\frac{dU}{dz}E_{ww}(k). \tag{8}$$

This budget is a balance between mechanical production (first term on the RHS) and energy redistribution through pressure-strain correlations (second and third terms on the RHS). The pressure-strain correlations are modeled with a standard spectral Rotta scheme. Its first component is a linear return-to-isotropy term with a Rotta constant $C_R \sim 1.8$ (slow part) and a characteristic timescale $\tau(k) = \epsilon^{-1/3}k^{-2/3}$ for $k \geq k_p$ and $\tau(k) = \epsilon^{-1/3}k_p^{-2/3}$ for $k < k_p$ (Katul et al., 2013). The second component is a nonlinear correction (Zeman & Tennekes, 1975) with characteristic constant $C_l = 3/5$ (called isotropization of the production). Note that the constant C_R used in the Rotta scheme is the same as for return-to-isotropy models used for the vertical velocity variance budget (see, e.g., Ayet, Katul, et al., 2020).

This budget has been successfully used (Katul et al., 2013) to model the observed co-spectrum in a neutral ASL. In this budget, the buoyancy source/sink term is neglected. This assumption follows from ASL measurements (the Kansas measurements; see Wyngaard, 2010; Wyngaard et al., 1971, page 233), scaling analysis in the inertial subrange, and direct numerical simulations (Katul et al., 2014).

From equation 8, the co-spectrum $F_{uw}(k)$ can be expressed as a function of the spectrum E_{ww}, and hence, the normalization condition (equation 7) reads

$$K = \frac{(1-C_l)}{C_R}\int_{2\pi a_i/z_i}^{2\pi a_s/d_s}\tau(k)E_{ww}(k)dk, \tag{9}$$

where $K = -\overline{u'w'}/(dU/dz)$ is the bulk turbulent viscosity. Using the idealized spectrum for $E_{ww}(k)$ presented in equation 5, the previous expression becomes

$$K_* = (zk_p)^{-4/3}\left\{\left[1-\frac{2\pi a_i z}{z_i}(zk_p)^{-1}\right]+\frac{3}{4}\left[1-\left(\frac{d_s}{2\pi a_s z}\right)^{4/3}(zk_p)^{4/3}\right]\right\}, \tag{10}$$

with $K_* = K\left(C_{ww}\epsilon^{1/3}z^{4/3}(1-C_l)/C_R\right)^{-1}$ a dimensionless turbulent viscosity that varies with atmospheric stability. This equation links zk_p to the bulk properties of the flow. It is comparable but not identical to equation 6 and, more importantly, it relies on a spectral budget (equation 8).

2.4. Dimensionless Variance and Stability Dependence

The dimensionless transition wavenumber zk_p has been linked to bulk properties of the flow: the dimensionless variance $\Sigma_* = \sigma_w^2(C_{ww}z^{2/3}\epsilon^{2/3})^{-1}$ and turbulent viscosity $K_* = K\left(C_{ww}\epsilon^{1/3}z^{4/3}(1-C_l)/C_R\right)^{-1}$. Those two bulk quantities are now expressed as a function of the stability parameter ζ using conventional MOST dimensionless functions (equation 3a,b) and estimates of TKE dissipation rate from equation 2.

The dimensionless variance Σ_* is given as

$$\Sigma_*(\zeta) = \frac{\kappa^{2/3}\phi_w(\zeta)}{C_{ww}(\phi_m - \zeta)^{2/3}}. \tag{11}$$

Accepted MOST dimensionless functions from the Kansas experiment (Kaimal & Finnigan, 1994; Sorbjan, 1989; see supporting information) are used to evaluate Σ_*. As shown in Figure 2b (solid line), the resulting Σ_* increases (resp. decreases) for unstable (resp. stable) conditions. The neutral value of Σ_* is 1.3, following the fact that $\phi_w(0) \sim 1.56$.

Similarly, the dimensionless turbulent viscosity can be expressed as a function of ζ and is given by

$$K_* = \frac{\kappa^{4/3}C_K}{C_{ww}\phi_m(\phi_m - \zeta)^{1/3}}, \tag{12}$$

where $C_K = C_R/(1-C_l)$. Its behavior (dashed line) is similar to Σ_*, even though its neutral value is of about 2.

3. Discussion

Equation 6 provides values of zk_p given the stability parameter ζ (that sets Σ_* through equation 11) and the two cutoff lengths d_s/a_s and z_i/a_i. In the following, it is assumed that the measurement height is small relative to the boundary layer height (i.e., $z/z_i \ll 1$) which, from equation 6, yields the following expression of zk_p:

$$zk_p(\zeta) = \left(\frac{5}{2}\right)^{3/2}\left[\Sigma_*(\zeta) + \frac{3}{2}\left(\frac{d_s}{2\pi a_s z}\right)^{2/3}\right]^{-3/2}. \tag{13}$$

While this approximation is valid in the ASL for a measurement height close to the surface, it can fail for measurements higher up in the atmospheric boundary layer or for very stable conditions (not considered here).

In this simplified model, the only remaining parameter that requires specification is $d_s/(a_s z)$. This parameter depends on the measuring properties of the instrument: the smallest wavelength sampled by the measuring device ($2\pi/d_s$) and its averaging and spectral filtering properties (a_s). An estimate of $d_s/(a_s z)$ may be obtained for neutral conditions by specifying a value of $zk_p(0)$ in equation 13. As discussed in section 1 and in Figure 1b, there is uncertainty in the value of zk_p for neutral conditions, which we use here to provide a range of values for $d_s/(a_s z)$.

Two limiting cases are considered: $k_p(0)z = 1$, as assumed in prior models (Katul et al., 2011), and a larger value $k_p(0)z = 1/\kappa \sim 1/0.4$ close to the estimates from the Kansas measurements (Kaimal et al., 1972; see the supporting information). Using equation 13 and the fact that $\Sigma_*(0) = 1.3$ (see Figure 2b) yields $d_s/(2\pi a_s z) = 0.71$ and $d_s/(2\pi a_s z) = 0.017$ for the first and second cases, respectively. Note that assuming a typical measurement height $z = 5$ m and an anemometer path length $d_s = 0.1$ m implies $a_s = 0.003$ and $a_s = 0.19$, respectively. In the first case (i.e., for $k_p(0)z = 1$), this corresponds to an effective cutoff wavenumber $2\pi a_s/d_s$ (i.e., including the spatial filtering properties of the instrument) three orders of magnitude larger than original instrument cutoff $2\pi/d_s$. This is a significant modulation, which questions the physical relevance of assuming $k_p(0)z = 1$ when using MOST dimensionless functions from the Kansas experiments to constrain Σ_*.

The modeled k_p *deviations* from the neutral value are now compared to reported measurements and estimates of k_p from several published ASL experiments. The estimates of this deviation, $k_p(\zeta)/k_p(0)$, are shown in Figure 3a and summarized in the supporting information. First, the widely used estimate of k_p from the Kansas experiment (Kaimal et al., 1972, measurements form 5 to 22 m on top of wheat stubble) is shown as

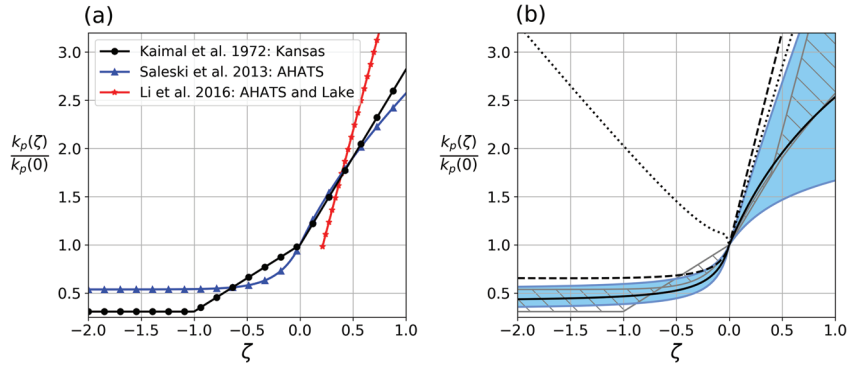

Figure 3. Relative transition wavenumber versus stability. (a) Experiments: spectral measurements from the Kansas experiment, estimates of the integral length scale from Salesky et al. (2013), and estimates of the Ozmidov length scale from Li et al. (2016). (b) Model predictions: matching between vertical variance and spectra (equation 13) for $k_p(0) = 1.6/z$ (solid black line) and for a range of values from $k_p(0) = 1/(\kappa z) = 2.5/z$ (upper blue line) to $k_p(0) = 1/z$ (lower blue line); matching between turbulent viscosity and co-spectra (equation 14) with a fixed return-to-isotropy set of constants (dashed line) and with a stability-dependent Rotta constant from Ayet, Katul, et al. (2020) (dotted line); envelope covering the data estimates of panel (a) (gray dashed area).

a black line. This estimate results from a direct determination of k_p as the wavenumber of the peak of the premultiplied vertical velocity spectra (as in Figure 1b). Second, the Advection Horizontal Array Turbulence Study (AHATS, z from 1 to 7 m on top of grass) provided an estimate of the streamwise integral lengthscale of the vertical velocity, which is inversely proportional to k_p (Salesky et al., 2013, blue lines). Finally, for moderately stable conditions ($0.3 < \zeta < 1$), Li et al. (2016) argued that the Ozmidov length scale should be the dominant scale for the turbulence spectra. The authors showed that replacing other estimates of k_p by the Ozmidov length scale in phenomenological models allowed explaining some of their caveats for mildly stable conditions. Being an additional estimate of the wavenumber of energy-containing eddies k_p, we show the Ozmidov length scale proposed by the authors on the basis of the AHATS data and of additional data above a lake in red.

The modeled variation of zk_p from equation 13 is shown in Figure 3b for the two limit values of $d_s/(a_s z)$ mentioned above (blue lines and shading). The trends are consistent with the expected increase (resp. decrease) of zk_p for stable (resp. unstable) conditions, which reflects the change, due to buoyancy, in the shape of the dominant eddies driving the vertical momentum flux (e.g., Katul et al., 2011). Variations of $d_s/(a_s z)$ allow testing the sensitivity of zk_p to changes in the large wavenumber cutoff and hence to changes in the neutral value $zk_p(0)$ (as seen in Figure 1b). As expected, the sensitivity is higher for stable than for unstable conditions. This results from σ_w^2 being lower for stable than for unstable conditions (and hence also Σ_*; see Figure 2). A change of $d_s/(a_s z)$ in equation 13 is thus larger relative to Σ_* for stable than for unstable conditions, causing a higher relative change in zk_p. In stable conditions, where the bulk variance is lower, the transition wavenumber is difficult to estimate, being sensitive to such measurement issues (as expected). Note that z/z_i was also varied over a reasonable range for the ASL ($z/z_i \leq 0.3$, not shown). The resulting variations of zk_p (from equation 6) were found significantly smaller than the variations induced by a change of $d_s/(a_s z)$.

Overall, the range of values obtained by varying $zk_p(0)$ (blue shadings) is larger than the range of values spanned by the data for stable conditions and similar to it for unstable conditions (gray hatches). For stable conditions, choosing $zk_p(0) \sim 1$ results in a poor estimate of the trend of zk_p, with respect to choosing $zk_p(0) \sim 1/\kappa$, closer to the Kansas data. This again hints towards the latter value of $zk_p(0)$ being more physical to describe ASL turbulence above a flat terrain. Nonetheless, the choice $zk_p(0) \sim 1/\kappa = 2.5$ (which is within the bounds of $zk_p[0]$ of Figure 1b, gray shadings) results in a relative deviation of k_p outside the envelope of the data (gray hatches in Figure 3b). Hence, the best match to the measurements was determined and is shown in black line in Figure 3b. It corresponds to $zk_p(0) = 1.6/z$ (and to $d_s/(2\pi a_s z) = 0.2$). The model falls close (for $-0.8 < \zeta < 0.5$) or within (for $\zeta \leq -0.8$ and $\zeta \geq 0.5$) the envelope of the data. More precisely, comparison between the AHATS estimates (blue line in Figure 3a) and the model (black line in Figure 3b) shows that it is correct up to a multiplicative factor of order one.

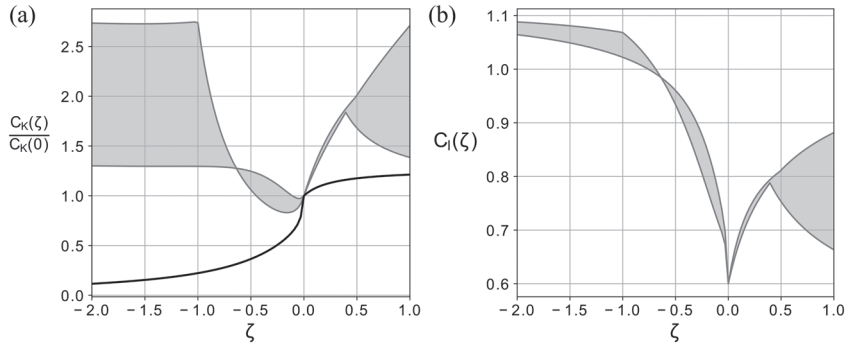

Figure 4. Return-to-isotropy constants versus stability. (a) Relative variation of $C_K = C_R/(1 - C_l)$ (i) required to match the data from Figure 3 (gray shadings) and (ii) by keeping C_l fixed and a stability-dependent C_R from Ayet, Katul, et al. (2020) (solid line); (b) gray shadings show the absolute variations of C_l required to match the data from Figure 3 if C_R is assumed to follow the stability-dependent variations consistent with (a), solid line.

The matching between the spectra and the vertical velocity variance offers an acceptable constraint to predict the relative variations of the transition wavenumber with ζ. This is ensured partly from the universality of the Kolmogorov constant C_{ww}. Instead, the matching between the co-spectra and the turbulent viscosity (equation 10) relies on two return-to-isotropy "constants," C_R and C_l whose universality for different conditions has been recently questioned. As mentioned earlier, C_R is also the return-to-isotropy constant used in the vertical velocity variance budget. In Ayet, Katul, et al. (2020) we have shown, using such a budget, that the value of the Rotta constant C_R should be revised to include stability-dependent effects. In the following, we extend this analysis to C_l, using the matching between the co-spectra and the turbulent viscosity and comparing it to the data of the transition wavenumber.

The transition wavenumber predicted from the matching between the co-spectra and the turbulent viscosity is obtained by setting $z/z_i \ll 1$ in equation 10:

$$zk_p(\zeta) = \left(\frac{7}{4}\right)^{3/4}\left[K_*(\zeta) + \frac{3}{4}\left(\frac{d_s}{2\pi a_s z}\right)^{2/3}\right]^{-3/4}, \tag{14}$$

where K_* depends, among others, on the ratio of the return-to-isotropy constants $C_K = C_R/(1 - C_l)$ which, for a neutral atmosphere, has a value of 4.5 (with $C_R = 1.8$ and $C_l = 3/5$). For a neutral atmosphere, we further assume, following Katul et al. (2013), that $d_s/(a_s z) = 0$. This results, using $K_*(0) \sim 2$ (see Figure 2), in $zk_p = (8/7)^{-3/4} = 0.9$, close to the expected unity value put forth in Townsend (1980). Katul et al. (2013) showed that this choice of d_s/a_s was required for the co-spectral model to recover the spectral properties of the ASL for neutral conditions.

As shown in Figure 3b (dashed line), the modeled transition wavenumber trend from equation 14 is in worse agreement with the data than equation 13. Since this matching depends on the value of C_K, this comparison suggests that C_K should be adjusted with respect to its neutral value of 4.5 to match zk_p. As a first adjustment, the stability dependence of C_R discussed in Ayet, Katul, et al. (2020) is included while maintaining $C_l = 3/5$ fixed (dotted line in Figure 3b). Even though for stable conditions the agreement with the data is improved, for unstable conditions the predicted behavior of zk_p is not consistent with its expected (and measured) decrease.

In fact, the variations of C_K needed to match the data of Figure 3a are an increase of C_K for mildly unstable and stable conditions (gray shadings in Figure 4a), which is inconsistent with the predicted decrease of C_R from Ayet, Katul, et al. (2020) (solid line in Figure 4a). Assuming that the stability dependence of C_R from Ayet, Katul, et al. (2020) also applies to the co-spectral budget (in Ayet, Katul, et al., 2020, it was derived for the budget of the vertical velocity), the only alternative left is that C_l should be stability dependent. The values of C_l needed to match the data of Figure 3a are shown as gray shadings in Figure 4b.

This co-spectral analysis shows that the timescales associated with the Rotta and nonlinear return-to-isotropy constants can be linked to the characteristic wavelength of the energy-containing spectrum (k_p), which is a physical result *per-se*. It also hints for revising the value of those constants for non-neutral conditions. Since the constant C_R is also used for return-to-isotropy modeling in the vertical

variance budget, this analysis also gives insights into the return-to-isotropy terms in such budgets, which are essential for numerical modeling (e.g., Canuto et al., 2001; Mellor & Yamada, 1982) and have been discussed in details in Bou-Zeid et al. (2018) and Ayet, Katul, et al. (2020).

4. Conclusion

An equation linking the bulk and spectral properties of the the vertical turbulent motions in the ASL was derived to predict the displacement of the transition wavenumber in the vertical velocity spectrum. The derived expression weakly depends on the atmospheric boundary layer height and instrument cutoff scale (d_s/a_s). The expression compared reasonably against multiple ASL measurements in a simplified framework where the effects of a finite boundary layer height were neglected. Besides improving the theoretical understanding of the ASL, this result also opens the path for several applications: (i) It can be used to diagnose the transition wavenumber from data sets measuring the bulk properties of the flow and hence help designing experiments where only large scale information or estimates about the flow are available; (ii) it can assist in building turbulent closures in numerical simulations by linking the bulk properties of the flow to that of energy-containing eddies (whose size is proportional to k_p; see, e.g., Gioia et al., 2010; Katul et al., 2011; Townsend, 1980).

To gain further insight on the physics controlling the transition wavenumber, an alternative link was studied, based on a co-spectral budget of turbulence. This second link involves constants controlling the timescale of return-to-isotropy of the flow. In accordance with the results of Ayet, Katul, et al. (2020), those constants should depend on stability to ensure a matching between the predicted transition wavenumber from the co-spectral framework and the data. A fair critique to the method used here is the choice of $\tau(k)$ (that only varies with ϵ) and the determination of ϵ from an equilibrated TKE budget. Not withstanding this critique, this second analysis establishes a physical link between the return-to-isotropy timescales and the transition wavenumber, which could lead to important insights on how external parameters (buoyancy, surface geometry, and large-scale forcings) can influence near-surface turbulence isotropy. This link will be elaborated upon in the future.

Data Availability Statement

The data used for Figure 1 can be found in Kaimal et al. (1972), Katul, Hsieh, and Sigmon (1997), Katul, Hsieh, Kuhn, et al. (1997), Katul and Chu (1998), and Katul et al. (2016). The data used for Figures 2–4 are described in the supporting information and in Kaimal et al. (1972), Salesky et al. (2013), and Li et al. (2016). The code used to generate the figures is available freely on Github (https://github.com/AAyet).

Acknowledgments
The authors thank the two anonymous reviewers for their insightful remarks. AA was supported by DGA grant No. D0456JE075, the French Brittany Regional Council, ANR Caravel, and ISblue project, Interdisciplinary graduate school for the blue planet (ANR-17-EURE-0015), co-funded by a grant from the French government under the program "Investissements d'Avenir." GGK was supported by the U.S. National Science Foundation (Grants NSF-AGS-164438, NSF-IOS-175489, and NSF-AGS-2028633).

References

Abid, R., & Speziale, C. (1993). Predicting equilibrium states with Reynolds stress closures in channel flow and homogeneous shear flow. *Physics of Fluids A: Fluid Dynamics*, *5*(7), 1776–1782. https://doi.org/10.1063/1.858852

Ayet, A., Chapron, B., Redelsperger, J.-L., Lapeyre, G., & Marié, L. (2020). On the impact of long wind-waves on near-surface turbulence and momentum fluxes. *Boundary-Layer Meteorology*, *174*(3), 465–491. https://doi.org/10.1007/s10546-019-00492-x

Ayet, A., Katul, G., Bragg, A., & Redelsperger, J. (2020). Scalewise return-to-isotropy in stratified boundary layer flows. *Journal of Geophysical Research: Atmospheres*, *125*, e2020JD032732. https://doi.org/10.1029/2020JD032732

Bonetti, S., Manoli, G., Manes, C., Porporato, A., & Katul, G. (2017). Mannings formula and Stricklers scaling explained by a co-spectral budget model. *Journal of Fluid Mechanics*, *812*, 1189–1212. https://doi.org/10.1017/jfm.2016.863

Bos, W., Touil, H., Shao, L., & Bertoglio, J.-P. (2004). On the behavior of the velocity-scalar cross correlation spectrum in the inertial range. *Physics of Fluids*, *16*(10), 3818–3823. https://doi.org/10.1063/1.1779229

Bou-Zeid, E., Gao, X., Ansorge, C., & Katul, G. (2018). On the role of return to isotropy in wall-bounded turbulent flows with buoyancy. *Journal of Fluid Mechanics*, *856*, 61–78. https://doi.org/10.1017/jfm.2018.693

Canuto, V. M., Howard, A., Cheng, Y., & Dubovikov, M. (2001). Ocean turbulence. Part I: One-point closure model – momentum and heat vertical diffusivities. *Journal of Physical Oceanography*, *31*(6), 1413–1426. https://doi.org/10.1175/1520-0485(2001)031<1413:OTPIOP>2.0.CO;2

Charuchittipan, D., & Wilson, J. (2009). Turbulent kinetic energy dissipation in the surface layer. *Boundary-Layer Meteorology*, *132*(2), 193–204. https://doi.org/10.1007/s10546-009-9399-x

Cuxart, J., Bougeault, P., & Redelsperger, J.-L. (2000). A turbulence scheme allowing for mesoscale and large-eddy simulations. *Quarterly Journal of the Royal Meteorological Society*, *126*, 1–30. https://doi.org/10.1002/qj.49712656202

Drobinski, P., Carlotti, P., Redelsperger, J.-L., Masson, V., Banta, R. M., & Newsom, R. K. (2007). Numerical and experimental investigation of the neutral atmospheric surface layer. *Journal of the Atmospheric Sciences*, *64*(1), 137–156. https://doi.org/10.1175/JAS3831.1

Foken, T. (2006). 50 years of the Monin–Obukhov similarity theory. *Boundary-Layer Meteorology*, *119*(3), 431–447. https://doi.org/10.1007/s10546-006-9048-6

Gioia, G., Guttenberg, N., Goldenfeld, N., & Chakraborty, P. (2010). Spectral theory of the turbulent mean-velocity profile. *Physical Review Letters*, *105*(18), 184501. https://doi.org/10.1103/PhysRevLett.105.184501

Grachev, A., Andreas, E., Fairall, C., Guest, P., & Persson, P. (2013). The critical Richardson number and limits of applicability of local similarity theory in the stable boundary layer. *Boundary-Layer Meteorology*, *147*(1), 51–82. https://doi.org/10.1007/s10546-012-9771-0
Hoxey, R., & Richards, P. (1992). Spectral characteristics of the atmospheric boundary layer near the ground. In *First UK wind engineering conference*. University of Cambridge.
Hsieh, C.-I., & Katul, G. G. (1997). Dissipation methods, Taylor's hypothesis, and stability correction functions in the atmospheric surface layer. *Journal of Geophysical Research*, *102*(D14), 16,391–16,405. https://doi.org/10.1029/97JD00200
Hunt, J., & Carlotti, P. (2001). Statistical structure at the wall of the high Reynolds number turbulent boundary layer. *Flow, Turbulence and Combustion*, *66*(4), 453–475. https://doi.org/10.1023/A:1013519021030
Kader, B., & Yaglom, A. (1990). Mean fields and fluctuation moments in unstably stratified turbulent boundary layers. *Journal of Fluid Mechanics*, *212*, 637–662. https://doi.org/10.1017/S0022112090002129
Kader, B., & Yaglom, A. (1991). Spectra and correlation functions of surface layer atmospheric turbulence in unstable thermal stratification. *Turbulence and Coherent Structures* (pp. 387–412). Dordrecht: Springer.
Kaimal, J., & Finnigan, J. (1994). *Atmospheric Boundary Layer Flows: Their Structure and Measurement*. Oxford, UK: Oxford University Press.
Kaimal, J., Wyngaard, J., Izumi, Y., & Coté, O. (1972). Spectral characteristics of surface-layer turbulence. *Quarterly Journal of the Royal Meteorological Society*, *98*(417), 563–589. https://doi.org/10.1002/qj.49709841707
Katul, G., Banerjee, T., Cava, D., Germano, M., & Porporato, A. (2016). Generalized logarithmic scaling for high-order moments of the longitudinal velocity component explained by the random sweeping decorrelation hypothesis. *Physics of Fluids*, *28*(9), 095104. https://doi.org/10.1063/1.4961963
Katul, G., & Chu, C.-R. (1998). A theoretical and experimental investigation of energy-containing scales in the dynamic sublayer of boundary-layer flows. *Boundary-Layer Meteorology*, *86*(2), 279–312. https://doi.org/10.1023/A:1000657014845
Katul, G., Hsieh, C.-I., Kuhn, G., Ellsworth, D., & Nie, D. (1997). Turbulent eddy motion at the forest-atmosphere interface. *Journal of Geophysical Research*, *102*, 13,409–13,421. https://doi.org/10.1029/97JD00777
Katul, G., Hsieh, C.-I., & Sigmon, J. (1997). Energy-inertial scale interactions for velocity and temperature in the unstable atmospheric surface layer. *Boundary-Layer Meteorology*, *82*(1), 49–80. https://doi.org/10.1023/A:1000178707511
Katul, G., Konings, A., & Porporato, A. (2011). Mean velocity profile in a sheared and thermally stratified atmospheric boundary layer. *Physical Review Letters*, *107*(26), 268502. https://doi.org/10.1103/PhysRevLett.107.268502
Katul, G., Porporato, A., Daly, E., Oishi, A., Kim, H.-S., Stoy, P., et al.(2007). On the spectrum of soil moisture from hourly to interannual scales. *Water Resources Research*, *43*, W05428. https://doi.org/10.1029/2006WR005356
Katul, G., Porporato, A., Manes, C., & Meneveau, C. (2013). Co-spectrum and mean velocity in turbulent boundary layers. *Physics of Fluids*, *25*(9), 091702. https://doi.org/10.1063/1.4821997
Katul, G., Porporato, A., & Nikora, V. (2012). Existence of k^{-1} power-law scaling in the equilibrium regions of wall-bounded turbulence explained by Heisenberg's eddy viscosity. *Physical Review E*, *86*(6), 066311. https://doi.org/10.1103/PhysRevE.86.066311
Katul, G., Porporato, A., Shah, S., & Bou-Zeid, E. (2014). Two phenomenological constants explain similarity laws in stably stratified turbulence. *Physical Review E*, *89*(2), 023007. https://doi.org/10.1103/PhysRevE.89.023007
Kolmogorov, A. (1941). The local structure of turbulence in incompressible viscous fluid for very large Reynolds numbers. *Proceedings of the USSR Academy of Sciences*, *30*, 301–305.
Launder, B., Reece, G. J., & Rodi, W. (1975). Progress in the development of a Reynolds-stress turbulence closure. *Journal of Fluid Mechanics*, *68*(3), 537–566. https://doi.org/10.1017/S0022112075001814
Li, D., Salesky, S., & Banerjee, T. (2016). Connections between the Ozmidov scale and mean velocity profile in stably stratified atmospheric surface layers. *Journal of Fluid Mechanics*, *797*, R3. https://doi.org/10.1017/jfm.2016.311
Lumley, J., & Newman, G. (1977). The return to isotropy of homogeneous turbulence. *Journal of Fluid Mechanics*, *82*(1), 161–178. https://doi.org/10.1017/S0022112077000585
Mellor, G., & Yamada, T. (1982). Development of a turbulence closure model for geophysical fluid problems. *Reviews of Geophysics*, *20*(4), 851–875. https://doi.org/10.1029/RG020i004p00851
Monin, A., & Obukhov, A. (1954). Basic laws of turbulent mixing in the surface layer of the atmosphere. *Proceedings of the Geophysical Institute of the USSR Academy of Sciences*, *24*(151), 163–187.
Moore, C. J. (1986). Frequency response corrections for eddy correlation systems. *Boundary-Layer Meteorology*, *37*(1–2), 17–35. https://doi.org/10.1007/BF00122754
Panchev, S. (1971). *Random Functions and Turbulence*, International Series of Monographs in Natural Philosophy (Vol. 32). Oxford, UK: Pergamon Press. https://doi.org/10.1016/C2013-0-02360-2
Redelsperger, J.-L., Mahé, F., & Carlotti, P. (2001). A simple and general subgrid model suitable both for surface layer and free-stream turbulence. *Boundary-Layer Meteorology*, *101*(3), 375–408. https://doi.org/10.1023/A:1019206001292
Rodier, Q., Masson, V., Couvreux, F., & Paci, A. (2017). Evaluation of a buoyancy and shear based mixing length for a turbulence scheme. *Frontiers in Earth Science*, *5*, 65. https://doi.org/10.3389/feart.2017.00065
Saddoughi, S., & Veeravalli, S. (1994). Local isotropy in turbulent boundary layers at high Reynolds number. *Journal of Fluid Mechanics*, *268*, 333–372. https://doi.org/10.1017/S0022112094001370
Salesky, S., Katul, G., & Chamecki, M. (2013). Buoyancy effects on the integral length scales and mean velocity profile in atmospheric surface layer flows. *Physics of Fluids*, *25*(10), 105101. https://doi.org/10.1063/1.4823747
Sorbjan, Z. (1989). *Structure of the Atmospheric Boundary Layer*. New Jersey: Prentice Hall. 551.51 SOR.
Taylor, G. (1922). Diffusion by continuous movements. *Proceedings of the London Mathematical Society*, *2*(1), 196–212.
Tchen, C. (1953). On the spectrum of energy in turbulent shear flow. https://doi.org/10.6028/jres.050.009
Townsend, A. (1980). *The Structure of Turbulent Shear Flow*. Cambridge, UK: Cambridge University Press.
Wyngaard, J. (2010). *Turbulence in the Atmosphere*. Cambridge, UK: Cambridge University Press.
Wyngaard, J., Coté, O., & Izumi, Y. (1971). Local free convection, similarity, and the budgets of shear stress and heat flux. *Journal of the Atmospheric Sciences*, *28*(7), 1171–1182. https://doi.org/10.1175/1520-0469(1971)028<1171:LFCSAT>2.0.CO;2
Zeman, O., & Tennekes, H. (1975). A self-contained model for the pressure terms in the turbulent stress equations of the neutral atmospheric boundary layer. *Journal of the Atmospheric Sciences*, *32*(9), 1808–1813. https://doi.org/10.1175/1520-0469(1975)032<1808:ASCMFT>2.0.CO;2